Journal of Engineering Mathematics **38:** 279–296, 2000.

Creation of spatial structure by an electric field applied to an ionic cubic autocatalator system

A.B. FINLAYSON and J.H. MERKIN
Department of Applied Mathematics, University of Leeds, Leeds, LS2 9JT, UK (e-mail: ABF: FINLAAB@spcs.britishsteel.co.uk; JHM: amtjhm@amsta.leeds.ac.uk)

Received 15 July 1999; accepted in revised form 23 December 1999

Abstract. The effects of applying electric fields to a reactor with kinetics based on an ionic version of the cubic autocatalator are considered. Three types of boundary condition are treated, namely (constant) prescribed concentration, zero flux and periodic. A linear stability analysis is undertaken and this reveals that the conditions for bifurcation from the spatially uniform state are the same for both the prescribed concentration and zero-flux boundary conditions, suggesting bifurcation to steady structures, whereas, for periodic boundary conditions, the bifurcation is essentially different, being of the Hopf type, leading to travelling-wave structures. The various predictions from linear theory are confirmed through extensive numerical simulations of the initial-value problem and by determining solutions to the (non-linear) steady state equations. These reveal, for both prescribed concentration and zero-flux boundary conditions, that applying an electric field can change the basic pattern form, give rise to spatial structure where none would arise without the field, can give multistability and can, if sufficiently strong, suppress spatial structure entirely. For periodic boundary conditions, only travelling waves are found, their speed of propagation and wavelength increasing with increasing field strength, and are found to form no matter how strong the applied field.

Key words: reaction-diffusion systems, ionic systems, electric-field effects, spatial structure, Turing bifurcations, cubic autocatalator

1. Introduction

Applying electric fields to ionic reacting chemical systems has been concerned mainly with travelling waves, with both pulse and front waves being considered. The former is exemplified by the excitable Belousov–Zhabotinsky (BZ) system, where both wave reversal and wave splitting have been observed in one-dimensional reactors [1]. In a two-dimensional configuration, wave breaking with spirals forming on the broken ends [2], spiral break up [3] and annihilation [4] and spiral drift [5, 6] have all been observed experimentally. These features have also been confirmed by numerical simulations of the appropriate models [2, 4, 5, 7, 8]. Experimental studies into the effects of electric fields on front waves have been based mostly on the iodate-arsenous acid system, with wave acceleration and deceleration as well as total wave annihilation being reported [9, 10]. Applying an electric field to this system has also been seen to affect the reaction selectivity mechanism resulting in qualitative changes in the waveform [11, 12]. Theoretical investigations into electric field effects on front waves have dealt extensively with ionic autocatalytic systems [13–17] with a variety of different structures being possible dependent mainly on the strength and direction of the applied field and the ratio of the diffusion coefficients of the reacting ionic species. The effects of applying an electric field on the lateral stabilty of planar front waves in ionic autocatalytic systems has also been discussed [18]. The result of all these studies is to show that the coupling of reaction and

diffusion with applied electric fields can, even in these kinetically simple systems, lead to a wide range of spatio-temporal behaviour.

There has been very much less attention directed towards understanding the effects that electric fields can have on pattern formation in reaction-diffusion systems. Ortoleva [19] originally suggested that the differential migration of ionic species resulting from the application of an electric field could modify and even destabilize an otherwise static structure. This possibility was clearly demonstrated in extensive numerical simulations of a system based on an ionic version of the Brusselator kinetic model [20, 21]. The electric field was seen to deform the pattern form (arising originally from a Turing Bifurcation as well as causing pattern splitting and coalescence. For stronger fields, coexistent regions with qualitatively different dynamics were seen to form, including regions of spatio-temporal chaos.

Here we consider this basic problem further by investigating the effects that an electric field can have on the spatial structures that arise in a model system based on an ionic version of Gray-Scott kinetics. We assume that the reaction is taking place within a backgound medium with a high ionic strength, enabling the constant field strength approximation to be made and the basic equations simplified. The previous studies [20, 21] used a variable electric field strength model, as derived for general ionic reacting systeml by [19, 22, 23]. We consider a one-dimensional reactor of finite length and three types of boundary conditions, namely prescribed concentrations, zero flux and periodic. We find that the conditions for bifurcations from the spatially uniform state, as given by a linear stability analysis, are the same for the prescribed concentration and zero flux cases. We show that applying an electric field can suppress the formation of spatial structure which would otherwise be generated through a Turing bifurcation, can alter the mode selection for the pattern and that spatial structure can arise with the electric field applied when it would not do so otherwise. With periodic boundary conditions the primary mechanism for pattern formation is found to be through a Hopf bifurcation. This results in the development of travelling waves. These form in any applied field, no matter how small when the system is capable of sustaining steady patterns without the electric field, and, when this is not the case, there is a minimum field strength above which travelling waves form. The implications of these linear stability conditions for pattern formation are then considered through numerical simulations of the full model.

2. The model

The ionic version of the cubic autocatalator model [24] that we consider is

$$P^+ \rightarrow A^+ \quad \text{rate } k_0 p_0, \tag{1}$$

$$A^+ + 2B^+ \rightarrow 3B^+ \quad \text{rate } k_1 a b^2, \tag{2}$$

$$B^+ \rightarrow C^+ \quad \text{rate } k_2 b, \tag{3}$$

with at least one further species Q^- present (though not taking part in the reaction) to maintain electroneutrality. The precursor species P^+ can be regarded as a relatively stable starting reactant which undergoes chemical transformation via two intermediate species A^+ and B^+ to the final inert product C^+. The initial concentrations of P^+ and Q^- are assumed to be very much greater than the maximum concentrations achieved by the intermediates. The neglect of precursor consumption in (1) can be justified by the 'pool chemical approximation' [25], so

that the concentration of P^+ can be taken as constant (at its initial concentration p_o) throughout. A full description of the derivation of the (non-ionic) cubic autocatalator model (1–3), as well as its behaviour as an oscillator (well-stirred system) and in the reaction-diffusion context, is given in [24].

With P^+ and Q^- present in excess, so that reactions (2, 3) make only a small net contribution to the overall ionic balance, we can invoke the constait field strength approximation used extensively in previous models (see [2, 4, 5, 7, 8], for example). A formal justification for making this approximation can be derive following closely that presented in [16, 17]. We assume that any spatial variations within the reactor can be represented adequately by a single longitudinal space variable. We make the equations governing the reaction, diffusion and electrochemical migration of reacting species A^+ and B^+ dimensionless using [25]

$$\left(\frac{k_2}{k_1}\right)^{1/2}, \quad \left(\frac{D_A}{k_2}\right)^{1/2}, \quad k_2^{-1}$$

as concentration, length and time scales respectively. This results in the dimensionless equations

$$\frac{\partial a}{\partial t} = \frac{\partial^2 a}{\partial x^2} - E\frac{\partial a}{\partial x} + \mu - ab^2, \tag{4}$$

$$\frac{\partial b}{\partial t} = D\frac{\partial^2 b}{\partial x^2} - DE\frac{\partial b}{\partial x} + ab^2 - b \tag{5}$$

on $0 < x < l, t > 0$, where l is the (dimensionless) length of the reactor and where

$$\begin{aligned} &D = \frac{D_B}{D_A}, \quad \mu = \frac{k_0 p_0}{k_2}\left(\frac{k_1}{k_2}\right)^{1/2} \text{(kinetic parameter)}, \\ &E = \frac{eF}{RT}\left(\frac{D_A}{k_2}\right)^{1/2} \text{(applied electric field)} \end{aligned} \tag{6}$$

are the dimensionless parameters. We can, without any loss in generality, assume that $E \geq 0$. Here D_A and D_B are the diffusion coefficients of A^+ and B^+ respectively, e is the (constant) applied electric field, T, F and R are temperature (assumed constant) and the Faraday and gas constants respectively.

Equations (4, 5) posses the spatially uniform stationary state $\mathcal{S} = \{(a, b) = (\mu^{-1}, \mu)\}$, which is temporally stable (*i.e.*, without diffusion or electromigration) for it $\mu > 1$ [25]. This leads us to apply the initial conditions

$$a = \mu^{-1}, b = \mu \quad \text{at } t = 0, 0 < x < l \tag{7}$$

perturbed slightly to allow for the formation of spatial structure (as described in the numerical simulations below). We consider three types of boundary conditions, namely

$$\text{Prescribed concentrations} : a = \mu^{-1}, b = \mu, \quad \text{at } x = 0, l, t > 0, \tag{8}$$

$$\text{Zero flux} : \frac{\partial a}{\partial x} = 0, \frac{\partial b}{\partial x} = 0, \quad \text{at } x = 0, l, t > 0, \tag{9}$$

$$\begin{aligned} &\text{Periodic} : a(0, t) = a(l, t), \quad b(0, t) = b(l, t), \\ &\frac{\partial a}{\partial x}(0, t) = \frac{\partial a}{\partial x}(l, t), \quad \frac{\partial b}{\partial x}(0, t) = \frac{\partial b}{\partial x}(l, t), \quad \text{for } t > 0. \end{aligned} \tag{10}$$

We are concerned here with the possibility that the combination of diffusion and electrochemical migration might destabilize the otherwise spatially uniform stationary state $\mathcal{S}$, so we restrict our attention to the case $\mu > 1$. We start by considering the effect of making a small perturbation to initial conditions (7).

3. Linear stability analysis

3.1. Prescribed concentrations

We consider small perturbations to $\mathcal{S}$ by putting $a = \mu^{-1} + A, b = \mu + B$, where A and B are small. Equations (4), (5) become, on linearization,

$$\frac{\partial A}{\partial t} = \frac{\partial^2 A}{\partial x^2} = -E\frac{\partial A}{\partial x} - \mu^2 A - 2B, \tag{11}$$

$$\frac{\partial B}{\partial t} = D\frac{\partial^2 B}{\partial x^2} - DE\frac{\partial B}{\partial x} + \mu^2 A + B, \tag{12}$$

subject to the boundary conditions

$$A = B = 0 \quad \text{at } x = 0, l, \quad t > 0. \tag{13}$$

To solve Equations (11), (12) we first express A and B in the form $A = \mathrm{e}^{Ex/2}\bar{A}$, $B = \mathrm{e}^{Ex/2}\bar{B}$. From (13) we still have $\bar{A} = \bar{B} = 0$ on $x = 0, l$ and Equations (11), (12) become

$$\frac{\partial \bar{A}}{\partial t} = \frac{\partial^2 \bar{A}}{\partial x^2} - \left(\frac{E^2}{4} + \mu^2\right)\bar{A} - 2\bar{B}, \tag{14}$$

$$\frac{\partial \bar{B}}{\partial t} = D\frac{\partial^2 \bar{B}}{\partial x^2} + \mu^2\bar{A} + \left(1 - \frac{DE^2}{4}\right)\bar{B}. \tag{15}$$

We look for a solution to Equations (14, 15) as

$$\begin{pmatrix} \bar{A} \\ \bar{B} \end{pmatrix} = \sum_{n=1}^{\infty} \begin{pmatrix} \alpha_n \\ \beta_n \end{pmatrix} e^{\omega_n t} \sin\left(\frac{n\pi x}{l}\right)$$

satisfying the boundary conditions on $x = 0, l$. Substitution in Equations (14, 15) then leads to the dispersion relation

$$\begin{aligned} \omega_n^2 + \left((1+D)(k_n^2 + \frac{E^2}{4}) + \mu^2 - 1\right)\omega_n + D\left(k_n^2 + \frac{E^2}{4}\right)^2 + (D\mu^2 - \\ -1)\left(k_n^2 + \frac{E^2}{4}\right) + \mu^2 = 0, \end{aligned} \tag{16}$$

where

$$k_n = \tfrac{n\pi}{l} (n = 1, 2, \dots).$$

3.2. Zero-flux boundary conditions

For the case of zero flux boundary conditions (9) we can still write $A = \mathrm{e}^{Ex/2}\bar{A}$, $B = \mathrm{e}^{Ex/2}\bar{B}$ in the linearized Equations (11), (12). Now we require

$$\frac{\partial \bar{A}}{\partial x} + \frac{E}{2}\bar{A} = 0, \quad \frac{\partial \bar{B}}{\partial x} + \frac{E}{2}\bar{B} = 0 \quad \text{at } x = 0, l. \tag{17}$$

This suggests that we looking for a solution in the form

$$\begin{pmatrix} \bar{A} \\ \bar{B} \end{pmatrix} = \sum_{n=1}^{\infty} \begin{pmatrix} \alpha_n \\ \beta_n \end{pmatrix} \mathrm{e}^{\omega_n t} \left[\cos\left(\frac{n\pi x}{l}\right) - \frac{El}{2n\pi} \sin\left(\frac{n\pi x}{l}\right) \right]$$

satisfying boundary conditions (17). Sustitution in Equations (14), (5) again gives dispersion relation (16).

We now consider dispersion relation (16) in more detail.

3.3. Neutral curves

The coefficient of ω_n in expression (16) is positive for all k_n (for $\mu > 1$) and so the only possibility for an instability is for $\omega_n = 0$ (saddle-node bifurcation). From (16) this occurs when

$$D\left(k_n^2 + \frac{E^2}{4}\right)^2 + (D\mu^2 - 1)\left(k_n^2 + \frac{E^2}{4}\right) + \mu^2 = 0, \tag{18}$$

from which it follows that we must have $D\mu^2 < 1$ (and hence $D < 1$ with $\mu > 1$). Condition (18) gives the neutral curves (the curves on which $\omega_n = 0$), the crossing of which as a parameter varies changes the stability of the spatially uniform steady state $\mathcal{S}$.

Equation (18) can be solved to get

$$k_n^2 + \frac{E^2}{4} = \frac{(1 - D\mu^2) \pm \sqrt{1 - 6D\mu^2 + D^2\mu^4}}{2D}. \tag{19}$$

Expression (19) requires $D\mu^2 \leq 3 - 2\sqrt{2}$ (with co-incident roots when $D\mu^2 = 3 - 2\sqrt{2}$). This is a necessary condition for a Turing bifurcation [26]. For $D\mu^2 < 3 - 2\sqrt{2}$, expression (19) represents a pair of straight lines in the (E^2, k_n^2)-plane. The situation is illustrated in Figure 1, where $X_{1,2}$ are given by

$$X_{1,2} = \frac{(1 - D\mu^2) \mp \sqrt{1 - 6D\mu^2 + D^2\mu^4}}{2D} \tag{20}$$

From Figure 1 we can see that, with $E = 0$ (for $D\mu^2 < 3 - 2\sqrt{2}$), the uniform steady state $\mathcal{S}$ can become unstable through a Turing bifurcation provided there is at least one integer n such that

$$X_1 < \frac{n^2\pi^2}{l^2} < X_2. \tag{21}$$

If this is the case, we may expect the exponential growth predicted by linear theory to be equilibrated at finite amplitude by the nonlinear terms and a pattern (a stable, spatially non-uniform steady state) to result [26]. The effect of applying an electric field can give rise to several possibilities. It may be possible to change the wavenumber k_n at which $\mathcal{S}$ becomes unstable, *i.e.* a value of k_n which lies inside the unstable region shown in Figure 1 with $E = 0$ may lie outside it when $E > 0$ while there could a value of another wavenumber which now lies inside the unstable region, whereas with $E = 0$ it did not. Also, it may be the case that

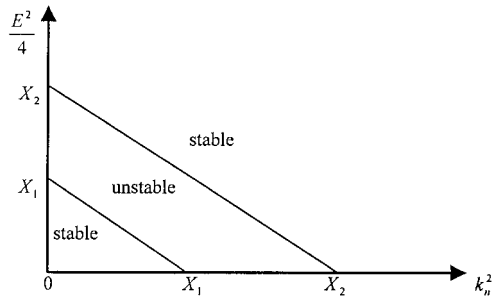

Figure 1. The neutral curves (where $\omega_n = 0$) as given by Equations (19,20) for $D\mu^2 < 3 - 2\sqrt{2}$, E^2 plotted against k_n^2, for both prescribed concentration and zero flux boundary conditions, X_1 and X_2 are given by (21). The regions where the spatially uniform state $\mathcal{S}$ is stable/unstable are shown.

there is no value of the wavenumber that lies inside the unstable region when $E = 0$ though with $E > 0$ there could be such a wavenumber. For sufficiently strong fields ($E^2 > 4X_2$) Figure 1 shows that $\mathcal{S}$ is stable to small perturbations with all wavenumbers. All this suggests that applying the electric field can change the basic pattern form, create spatial structure when none exists without the field or suppress pattern formation altogether. Finally, we note that applying an electric field cannot alter the inherent stability of $\mathcal{S}$ if $D\mu^2 > 3 - 2\sqrt{2}$, in which case $\Re(\omega_n)$ remains negative for all E. We examine these predictions from linear theory by obtaining numerical soultions of the full initial-boundary-value problem (4-9), but before doing so we consider the case when the periodic boundary conditions (10) are applied.

3.4. Periodic boundary conditions

A solution to the linearized Equations (11), (12) satisfying the periodic boundary conditions (10) can be expressed in the form

$$\begin{pmatrix} A \\ B \end{pmatrix} = \sum_{n=1}^{\infty} e^{\omega_n t} \left[\begin{pmatrix} a_n \\ b_n \end{pmatrix} \cos\left(\frac{2n\pi x}{l}\right) + \begin{pmatrix} c_n \\ d_n \end{pmatrix} \sin\left(\frac{2n\pi x}{l}\right) \right].$$

Substitution in Equations (11, 12), equating terms in $\cos((2n\pi x)/l)$ and $\sin((2n\pi x)/l)$, and requiring that the resulting linear algebraic equations for the coefficients a_n, b_n, c_n and d_n have a nontrivial solution leads to a dispersion relation which is now a quartic in ω_n, namely

$$\omega_n^4 + A_0\omega_n^3 + B_0\omega_n^2 + C_0\omega_n + D_0 = 0, \tag{22}$$

where

$$A_0 = 2\left[(1+D)\kappa_n^2 + \mu^2 - 1\right] > 0,$$

$$B_0 = \left[(D+1)\kappa_n^2 + \mu^2 - 1\right]^2 + 2\left[D\kappa_n^4 - (1 - D\mu^2)\kappa_n^2 + \mu^2\right] + E^2\kappa_n^2(1+D^2),$$

$$C_0 = \left[(D+1)\kappa_n^2 + \mu^2 - 1\right]\left[D\kappa_n^4 - (1 - D\mu^2)\kappa_n^2 + \mu^2\right] + 2E^2\kappa_n^2\left(D(D+1)\kappa_n^2 + \right.$$
$$\left. + D^2\mu^2 - 1\right),$$

$$D_0 = D^2\kappa_n^4E^4 + \kappa_n^2E^2[2D^2\kappa_n^4 - 2D(1 - D\mu^2)\kappa_n^2 + 1 - 4D\mu^2 + D^2\mu^4] +$$
$$+ [(\kappa_n^2 + \mu^2)(D\kappa_n^2 - 1) + 2\mu^2]^2$$

and where the wavenumber is now $\kappa_n = (2n\pi)/l$ $(n = 1, 2, \dots)$.

We first consider the possibilty of having saddle-node bifurcations with $E > 0$ through ω_n being zero. This requires that the coefficient D_0 in Equation (22) be zero, which can be possible only if the coefficient of E^2 in this expression is negative. We can write the condition that $D_0 = 0$ in the form

$$\left[D\kappa_n^2 E^2 + \left(D\kappa_n^4 - (1 - D\mu^2)\kappa_n^2 + \mu^2\right)\right]^2 + (1 - 6D\mu^2 + D^2\mu^4)\kappa_n^2 E^2 = 0, \tag{23}$$

from which it follows that a necessary condition to have $D_0 = 0$ is that $3 - 2\sqrt{2} < D\mu^2 < 3 + 2\sqrt{2}$. If we now regard Equation (23) as a quadratic equation for E^2 and calculate the discriminant Δ, we find that

$$\Delta = \left[2D\kappa_n^2 - 1 + D\mu^2\right]^2 \left(1 - 6D\mu^2 + D^2\mu^4\right). \tag{24}$$

Expression (24) is negative for $D\mu^2$ in the range $3 - 2\sqrt{2} < D\mu^2 < 3 + 2\sqrt{2}$ and hence there are no real roots in this case and we cannot have a bifurcation with $\omega_n = 0$. The only possibility is to have $E = 0$. From the dispersion relation (22) and expression (23) we can see that $\omega_n = 0$ (with $E = 0$) when

$$D\kappa_n^4 - (1 - D\mu^2)\kappa_n^2 + \mu^2 = 0, \tag{25}$$

which recovers the condition for a Turing bifurcation given previously [26], namely that, for $D\mu^2 < 3 - 2\sqrt{2}$, a Turing bifurcation will arise with $E = 0$ provided there is at least one integer in the range $X_1 < (4n^2\pi^2)/(1/l^2)X_2$ (where X_1, X_2 are given by (20)). The above establishes that $D_0 > 0$ for $E > 0$ for all D and μ.

We next consider the possibility of having a Hopf bifurcation. This will occur when ω_n is purely imaginary and to determine the curves in (E^2, κ_n)-space on which this will occur we put $\omega_n = i\alpha_n (\alpha_n$ real). Substitution in Equation (22), equating real and imaginary parts and then eliminating α_n. We obtain the condition for a Hopf bifurcation as

$$C_0^2 - A_0 B_0 C_0 + A_0^2 D_0 = 0, \tag{26}$$

where A_0, B_0, C_0 and D_0 have been given above. Relation (26) can be expressed as a quadratic equation in E^2 as

$$a_0\kappa_n^4 E^4 + b_0\kappa_n^2 E^2 + c_0 = 0, \tag{27}$$

where

$$a_0 = (1 - D)^2(1 + D)^2(\mu^2 + \kappa_n^2)(1 - D\kappa_n^2),$$

$$b_0 = -2\left[(1 + D)\kappa_n^2 + \mu^2 - 1\right]^2 \left((D^2 + 1)(D\kappa_n^4 - (1 - D\mu^2)\kappa_n^2 + \mu^2) - (1 - D^2\mu^2\right),$$

$$c_0 = -\left[(1 + D)\kappa_n^2 + \mu^2 - 1\right]^4 \left(D\kappa_n^4 - (1 - D\mu^2)\kappa_n^2 + \mu^2\right).$$

Clearly Equation (27) requires $D \neq 1$. Equation (27) can be solved to give, after some algebra, the roots

$$E_1^2 = \frac{((1 + D)\kappa_n^2 + \mu^2 - 1)^2(D\kappa_n^4 - (1 - D\mu^2)\kappa_n^2 + \mu^2)}{(1 - D)^2\kappa_n^2(1 - D\kappa_n^2)(\mu^2 + \kappa_n^2)}, \quad (D \neq 1) \tag{28}$$

$$E_2^2 = -\frac{((1 + D)\kappa_n^2 + \mu^2 - 1)^2}{(1 + D)^2\kappa_n^2}. \tag{29}$$

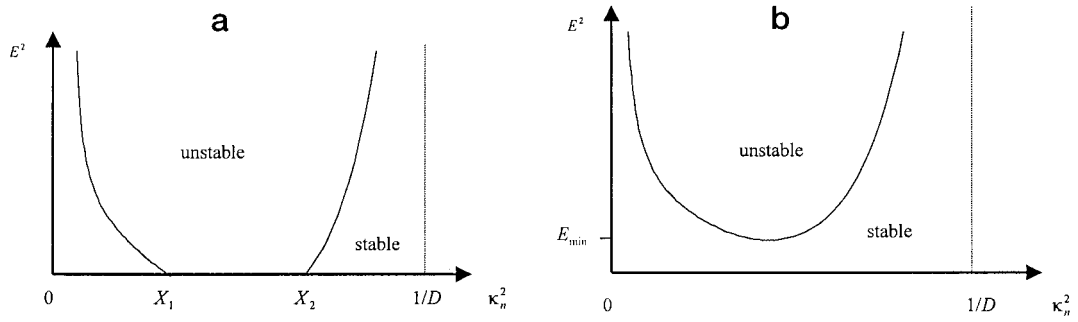

Figure 2. Hopf bifurcation curves for periodic boundary conditions, E_1^2 plotted against κ_n^2 as given by Equation (29) for the cases (a) $D\mu^2 < 3-2\sqrt{2}$, where X_1 and X_2 are given by expression (21) and (b) $D\mu^2 > 3-2\sqrt{2}$, showing the strictly positive minimum value of E below which $\mathcal{S}$ is stable for all wavenumbers.

Clearly it is only the root E_1^2 as given by (28) that is required. If $D\mu^2 < 3 - 2\sqrt{2}$ (so that Turing bifurcations are possible with $E = 0$) the numerator in (28) is negative for $X_1 < \kappa_n^2 < X_2$ (again X_1, X_2 are given by (20)) and positive otherwise. The Hopf bifurcation curve has vertical asymptotes at $\kappa_n^2 = 0$ and at $\kappa_n^2 = 1/D$ (note that $X_2 < 1/D$). The curve has the form shown in Figure 2a in this case. If $D\mu^2 > 3 - 2\sqrt{2}$, $(D \neq 1)$, the numerator is positive for all κ_n^2 and the the Hopf bifurcation curve has the form shown in Fogure 2b. In this case there is a (strictly positive) minimum value of E below which $\mathcal{S}$ is stable for all wavenumbers. The bifurcation curve shown in Figure 2b is similar in form to that derived by Satnoianu *et al.* [27, 28] for a related problem. There are no solutions to Equation (28) for $D = 1$, since, in this case, $a_0 = 0$ and b_0 and c_0 are both negative.

We can interpret the graphs shown in Figure 2 as follows. If the system supports a Turing bifurcation with $E = 0$, then the steady state $\mathcal{S}$ remains unstable with $E > 0$. However, with $E > 0$ the primary bifurcation is now a Hopf bifurcation, as opposed to the saddle-node bifurcation for the Turing instability, and this results in the steady stuctures with $E = 0$ becoming travelling waves propagating in the system for $E > 0$. If the system cannot support a Turing bifurcation with $E = 0$ then there is a (strictly positive) threshold value of the applied electric field above which $\mathcal{S}$ may become unstable. This can happen with $D\mu^2 < (3 - 2\sqrt{2})$ and there being no wavenumber κ_n such that $X_1 < \kappa_n^2 < X_2$ (Figure 2a) or when $D\mu^2 > (3 - 2\sqrt{2})$. This latter case requires κ_1^2 (at least) to be such that $\kappa_1^2 < 1/D$ or equivalently $l > 2\pi\sqrt{D}$ (Figure 2b). If this is the case then $\mathcal{S}$ becomes unstable through a Hopf bifurcation (again to travelling waves) for all applied field strengths $E > E_{\min}$ where $E_{\min} = \min\{E_1(\kappa_i^2) = \kappa_i^2 < 1/D\}$.

We now test the various predictions obtained from our linear stability analysis by numerical simulations of the full initial-value problem (4,5).

4. Numerical simulations

The initial-boundary-value problem (4,5,8) was solved numerically by use of a standard implicit method, based on the Crank-Nicolson scheme, for integrating parabolic equations, see [29] for more details. Boundary conditions (8) or (9) were implemented in the usual way and only a slight modification was required to account for the periodic conditions (10). We transformed the spatial domain from $0 < x < l$ to $0 < X < 1$ by putting $X = \frac{x}{l}$ and the

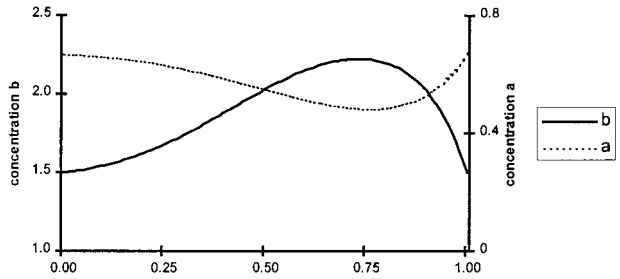

Figure 3. Concentration profiles for a and b obtained at large times from the numerical integration of initial-boundary-value problem (4, 5, 8) for $E = 4{\cdot}0$, $l = 2{\cdot}0$ and $D = 0{\cdot}0674$, $\mu = 1{\cdot}5$.

results are presented in terms of X. A small local perturbation was made to the initial state $\mathcal{S}$ and this was followed as it evolved in time. The results presented below are for the large-time behaviour when transient effects have died out and when the system has reached a steady state or some other clearly defined time varying structure. We treat the three cases in turn.

4.1. PRESCRIBED CONCENTRATION

We took fixed values for μ and D, namely $\mu = 1{\cdot}5$, $D = 0{\cdot}0674$, so that $D\mu^2 < (3 - 2\sqrt{2})$, and examined how the solution evolved for different values of l and E. For these parameter values $X_1 = 3{\cdot}7986$ and $X_2 = 8{\cdot}7882$. In all cases we found that the solution approached a steady state for t large and this is what we concentrate on.

We start by considering the case $l = 2{\cdot}0$. Here $k_1^2 < X_1$ and $\frac{2}{2} > X_2$ so there is no Turing bifurcation with $E = 0$. It is only the k_1-mode that can become unstable for $E > 0$ and this mode lies in the unstable region for E in the range $E_1^{(1)} = 2{\cdot}3075 < E < 5{\cdot}0282 = E_2^{(1)}$, where we use the notation $E_i^{(n)}$ to denote where the k_n-mode crosses the neutral curves $E^2/4 = X_i - k_n^2$, $i = 1, 2$ (see Figure 1). For values of $0 < E < E_1^{(1)}$ and $E > E_2^{(1)}$ we found that the initial perturbation produced some short-time transient behaviour in which a spatial structure formed before dying away, with the system returning to the spatially uniform state $\mathcal{S}$. For values of E in the range $E_1^{(1)} < E < E_2^{(1)}$ a stable steady spatial structure formed, as predicted from linear theory. This is illustrated in Figure 3, where we give large time plots of the concentrations a and b for $E = 4{\cdot}0$. This pattern has a single turning point associated with the k_1-mode and shows a marked skew in the direction of the electric field.

We next considered the case where there was a Turing bifurcation with $E = 0$, taking $l = 6{\cdot}0$. In this case both the k_4 and k_5-modes are unstable with $E = 0$ and it is the k_5-mode that is selected from our initial perturbation, as can be seen in Figure 4a (for $E = 0$). (Figures 4 give plots of b at large times for this case.) In Figures 4b-e we illustrate the change in the pattern form as the electric field strength E is increased. Figure 4b ($E = 2{\cdot}828$) shows an increase/decrease in the maximum/minimum concentrations, with the k_4-mode now appearing to be the most unstable mode ($E_2^{(5)} = 2{\cdot}7816$ is less than this value of E and so we could expect a change in the dominant mode). There is also a skewing of the pattern in the direction of the electric field (compare with Figure 4a). This trend continues for increased E (Figures 4c and 4d for $E = 4{\cdot}0$ and $E = 4{\cdot}899$ respectively). Figures 4c,d show that relatively large concentrations of B^+ can be achieved in the pattern and that, as E is increased, the next (k_3-mode) is selected ($E_2^{(4)} = 4{\cdot}1961$). On further increasing E, we approach the upper stability boundary at $E_2^{(1)} = 5{\cdot}8358$, as is evident in Figure 4e (for $E = 5{\cdot}2915$). In this case the

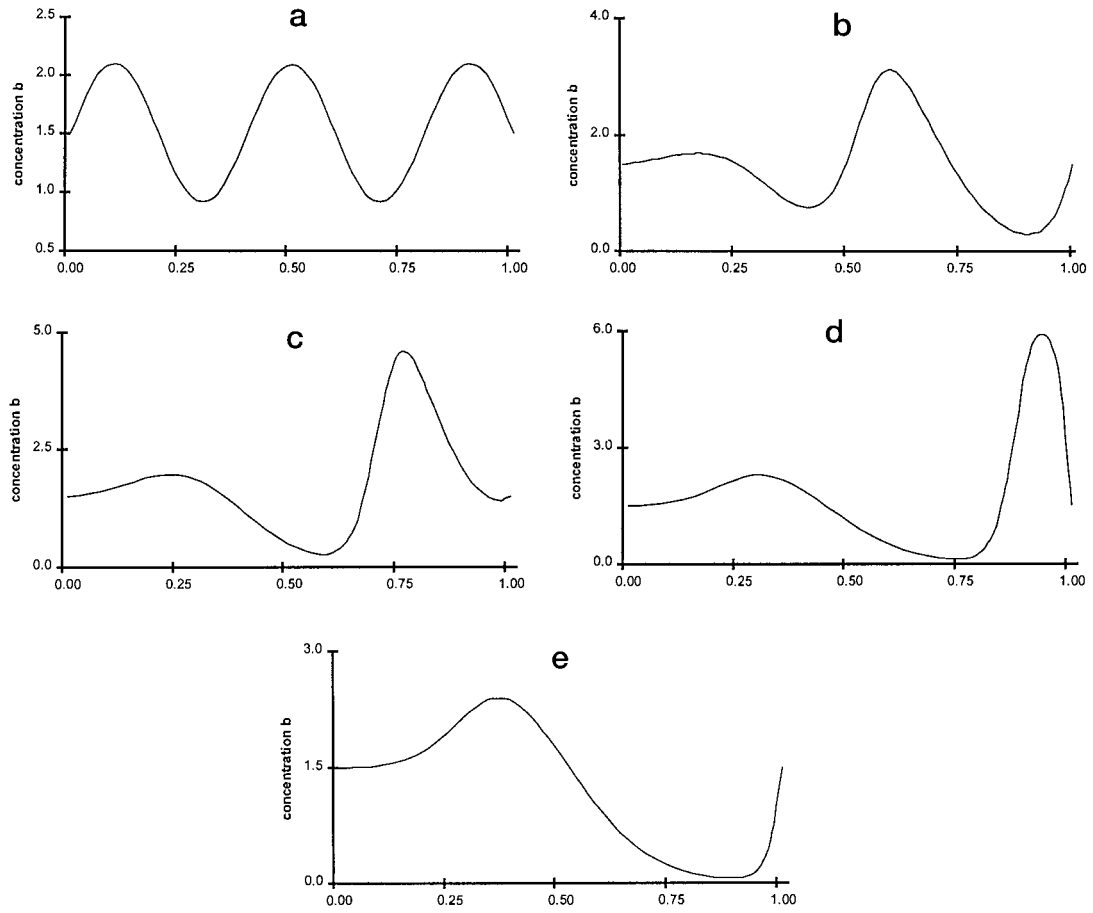

Figure 4. Concentration profiles for b obtained at large times from the numerical integration of initial-boundary-value problem (4, 5, 8) for $D = 0{\cdot}0674$, $\mu = 1{\cdot}5$, $l = 6{\cdot}0$ and (a) $E = 0{\cdot}0$, (b) $E = 2{\cdot}828$, (c) $E = 4{\cdot}0$, (d) $E = 4{\cdot}899$, (e) $E = 5{\cdot}2915$.

maximum deviations from $\mathcal{S}$ are reduced from those seen in Figure 4d and it is the k_2-mode that appears to be selected. A feature to note about the patterns for E close to $E_2^{(1)}$ is that both $((\partial a)/(\partial x))_{x=0}$ and $(\partial b)/(\partial x))_{x=0}$ become very small.

We find that stable patterns arise for values of E slightly greater than $E_2^{(1)}$, up to $E \simeq 5{\cdot}9$ in the present case. These patterns are similar to those shown in Figure 4e, with the maximum concentration of B^+ being slightly reduced and both $((\partial a)/(\partial x))_{x=0}$ and $((\partial b)/(\partial x))_{x=0}$ becoming smaller. For larger values of E than these there is transient behaviour whereby a structure similar to that seen Figure 4e is rapidly formed. This then propagates slowly in the direction of the field towards the $X = 1$ boundary, where it leaves the system which finally returns to the spatially uniform state $\mathcal{S}$.

All the results described above resulted from a perurbation localised close to $X = 0$. We tried different locations for the initial perturbation to $\mathcal{S}$ and found that the form that the resulting pattern took could depend on the location of this perturbation. We illustrate this by comparing the patterns which arise from perturbing $\mathcal{S}$ close to the $X = 1$ boundary for $E = 4{\cdot}0$ and $l = 6{\cdot}0$. This is shown in Figure 5 to compare with Figure 4c. These results suggest that the system is capable of sustaining different stable spatial structures for the same

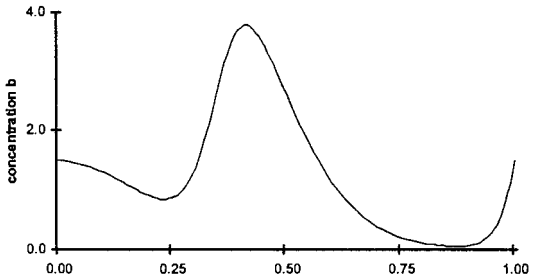

Figure 5. Concentration profiles for b obtained at large times from the numerical integration of initial-boundary-value problem (4, 5, 8) for $E = 4{\cdot}0, l = 6{\cdot}0, D = 0{\cdot}0674, \mu = 1{\cdot}5$ with the initial perturbation close to the $X = 1$ boundary. This illustrates the dependence of the final pattern on the location of the initial perturbation, compare with Figure 4c.

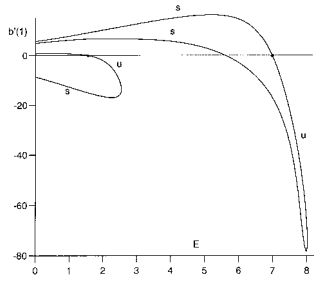

Figure 6. Bifurcation diagram, a plot of $b_1 \equiv b'(1)$ against E obtained from the numerical solution of the steady versions of Equations (4, 5, 8), for $\mu = 1{\cdot}5, D = 0{\cdot}05, l = 2{\cdot}0$. The bifurcations from small amplitude at $E_1^{(1)}$ and $E_2^{(1)}$ are shown by •.

set of parameter values. We next examine this point, and the possibility of having patterns for values of $E > E_2^{(1)}$ further by determining $(a(x), b(x))$, the solutions to the steady versions of Equations (4,5,8).

4.1.1. *Bifurcation Diagram*

We determined $(a(X), b(X))$ (where $X = x/l$) by solving the steady versions of Equations (4,5,8) numerically using a standard boundary-value problem solver. The results are presented in terms of plots of $b_1 \equiv b'(1)$ against E (for given values of the other parameters). We consider a case where Turing structures are possible with $E = 0$, namely $\mu = 1{\cdot}5, D = 0{\cdot}05, l = 2{\cdot}0$. For these values $X_1 = 3{\cdot}0642$ and $X_2 = 14{\cdot}6858$ so that it is only the k_2-mode which is unstable for $E = 0$. The results are shown in Figure 6.

This figure shows two distinct sets of solutions for $E \geq 0$, with both bifurcations from small amplitude at $E_1^{(1)}$ and $E_2^{(1)}$ being transcritical bifurcations (located on Figure 6 by •). The bifurcation from small amplitude at $E_2^{(1)} = 6{\cdot}991$ produces a solution branch for $E < E_2^{(1)}$, giving a finite amplitude pattern at $E = 0$, with the k_2-mode being the dominant mode for this branch. The transcritical bifurcation at $E_2^{(1)}$ also produces a solution branch in $E > E_2^{(1)}$. This undergoes a saddle-node bifurcation at $E = 8{\cdot}0186$ leading to a further branch for $E < E_2^{(1)}$, which also has a finite amplitude pattern at $E = 0$. This second solution branch crosses the $b_1 = 0$ axis at $E = 5{\cdot}601$, where there is still a finite amplitude pattern, and corresponds to the change in dominant mode from k_2 to k_1. The stability of these solution branches, as obtained from numerical integrations of initial-boundary-value problem (4, 5, 8) from different initial perturbations, are indicated on the figure.

The transcritical bifurcation from small amplitude at $E = E^{(1)} = 1{\cdot}545$ gives solution branches in which the k_1-mode is dominant throughout. The solution branch in $E > E_1^{(1)}$ arising from this bifurcation has a further saddle-node bifurcation at $E = 2{\cdot}534$ resulting in another two finite amplitude patterns at $E = 0$. The stability of these solution branches, again obtained from numerical integrations of Equations (4, 5, 8), is also indicated on Figure 6. The main features to note from the bifurcation diagram shown in Figure 6 is that (up to three)

different stable patterns are possible for the same parameter values and that there is an upper bound on the electric field strength E for the existence of these patterns.

4.2. ZERO FLUX

Here we took the same parameter values as for the prescribed concentration case when there is a Turing bifurcation at $E = 0$, namely $\mu = 1{\cdot}5$, $D = 0{\cdot}0674$, $l = 6{\cdot}0$ and solved initial-boundary-value problem (4,5,9) numerically for a range of values of E. The results are shown in Figure 7 as profile plots of the concentration b at sufficiently large times for these to have become steady. A similar picture to that seen previously emerges. For $E = 0$ (Figure 7a) the k_5-mode is the dominant one. The dominant unstable mode changes as E is increased with the patterns having fewer turning points and much larger concentrations of B^+ being attained. A further feature to note about the patterns shown in Figure 7 is the region close to the $X = 1$ boundary where the autocatalyst B^+ is almost entirely removed (see especially Figures 7b,c). For the larger values of E (Figures 7d,e) the concentration profile of B^+ close to the $X = 0$ boundary becomes flat, at its spatially uniform value of $b = 1{\cdot}5$, even though large excursions from this value are seen towards the $X = 1$ boundary. As in the previous case, the particular pattern to which the system settles at large t depends on the nature of the initial perturbation, with different patterns being possible at the same parameter values, as will be confirmed in the bifurcation diagram we describe below for zero flux boundary conditions. Finally we note that for sufficiently large field strengths pattern formation was fully suppressed and only the spatially uniform state $\mathcal{S}$ appeared as the long-time behaviour.

4.2.1. *Bifurcation Diagram*

The steady-state versions of situations (4,5,9) were integrated numerically by means of a standard boundary-value problem solver for $D = 0{\cdot}05$, $\mu = 1{\cdot}5$, $l = 2{\cdot}0$. The results are shown in Figure 8 as plots of $b(1)$ against E. As these are the same parameter values as for Figure 6, (I) = $E_1^{(1)}$ and $E_2^{(1)}$ take the same values, namely $E_1^{(1)} = 1{\cdot}545$, $E_2^{(1)} = 6{\cdot}991$ (shown by $\bullet$). Again the bifurcations at small amplitude from $E_1^{(1)}$ and $E_2^{(1)}$ are transcritical bifurcations, though here the picture is somewhat more complex than that shown in Figure 6. Now it is possible to have up to six different solutions for the same set of parameters (*e.g.* at $E = 2{\cdot}5$), though not all these are stable. (The stability of the various solution branches is indicated on the figure.) There are now just two (only one being stable) finite amplitude patterns at $E = 0$ and again nontrivial solutions exist for $E > E_2^{(1)}$, up to the saddle-node bifurcation at $E = 8{\cdot}0199$. The existence of a range of E over which for one stable solution branch $b(1)$ is almost zero can be seen (compare with Figures 7b,c) and the stable solutions corresponding to high values of $b(1)$ for $E > 6{\cdot}5$ have $b(0) \simeq 1{\cdot}5$ (compare with Figures 7d,e). The important points to note from Figure 8 are that multiple stable patterns (up to 4) are possible and that there is an upper bound on E for the existence of stable patterns, which is slightly greater than the upper bifurcation value predicted from linear theory.

We now turn to the case of periodic boundary conditions, where linear theory predicts qualitatively different behaviour.

4.3. PERIODIC BOUNDARY CONDITIONS

We consider two cases, namely one where there is a Turing bifurcation with $E = 0$, which necessitates having $D < 1$, and a case where $D > 1$, for which there can be no Turing bifurcation with $E = 0$ and a strictly positive value for E is needed to give an instability

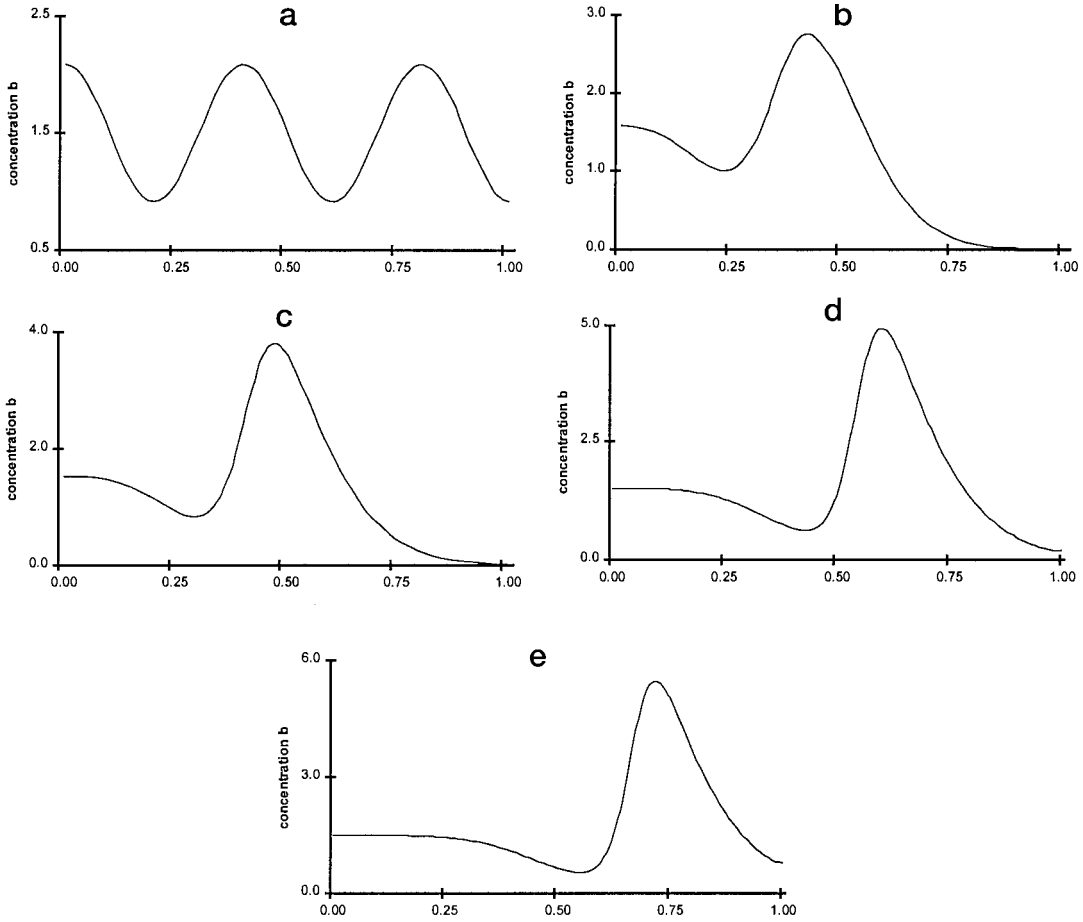

Figure 7. Concentration profiles for b obtained at large times from the numerical integration of initial-boundary-value problem (4, 5, 9) (zero flux boundary conditions) for $D = 0{\cdot}0674$, $\mu = 1{\cdot}5$, $l = 6{\cdot}0$ and (a) $E = 0{\cdot}0$, (b) $E = 2{\cdot}828$, (c) $E = 4{\cdot}0$, (d) $E = 4{\cdot}899$, (e) $E = 5{\cdot}2915$.

(Figure 2b). For each case we took $\mu = 1{\cdot}5$ and then $D = 0{\cdot}0674$, $l = 20{\cdot}0$ for the first case and $D = 10{\cdot}0$, $l = 100{\cdot}0$ for the second case.

The results for the first example are shown in Figuere 9 as grey-level contour plots of b. This sequence of figures shows the steady Turing pattern with $E = 0$ (Figure 9a) and the development of travelling waves for $E > 0$, travelling waves were found to develop for all the values of $E > 0$ tried, no matter how small, confirming the predictions from linear theory. Figures 9b (for $E = 2{\cdot}828$) and 9c (for $E = 6{\cdot}0$) show that the number of waves on the interval $0 \leq x \leq l$ decreases as E increases, from 8 waves with $E = 0$ to 5 waves (Figure 9b) and 3 waves Figure 9c). For these values of E, the waves propagate to the left with speeds computed from the numerical integrations of $v = -0{\cdot}085$ and $v = -0{\cdot}081$, respectively. As E is increased further, Figure 9d for $E = 6{\cdot}8556$, the wave speed has decreased considerably from that shown in Figure 9c, to $v = -0{\cdot}0085$. For slightly higher values of E (Figure 9e for $E = 7{\cdot}071$, where $v = 0{\cdot}009$) the direction of propagation changes and the waves now travel to the right, with a speed which increases with E (Figure 9f for $E = 11{\cdot}0$, where $v = 0{\cdot}106$).

For $D = 10{\cdot}0$ (and $\mu = 1{\cdot}5$) the turning point on the neutral curve gives $E_{\min} = 1{\cdot}849$, at $\kappa^2 = 0{\cdot}029$, (see Figure 2b). With $l = 100$ the first mode to go unstable is κ_3 at $E = 1{\cdot}908$

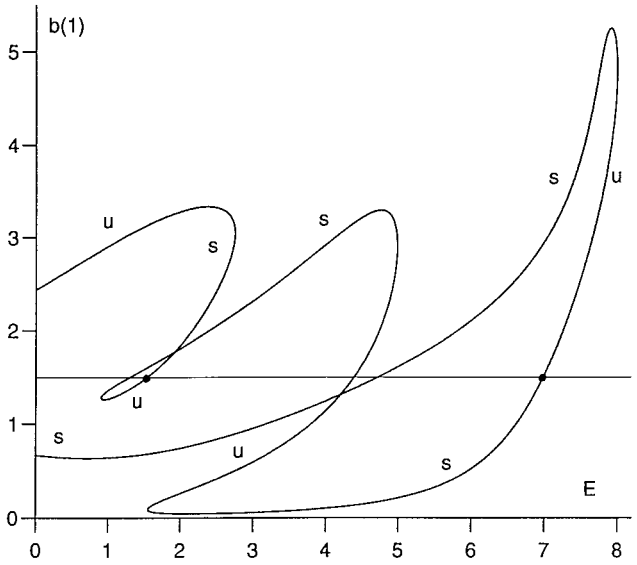

Figure 8. Bifurcation diagram, a plot of $b(1)$ against E obtained from the numerical solution of the steady versions of Equations (4, 5, 9) (zero flux boundary conditions), for $\mu = 1{\cdot}5$, $D = 0{\cdot}05$, $l = 2{\cdot}0$. The bifurcations from small amplitude at $E_1^{(1)}$ and $E_2^{(1)}$ are shown by •.

(the κ_2 and the κ_4 modes become unstable at $E = 2{\cdot}216$ and $E = 3{\cdot}179$, respectively). For this case we found that all the travelling waves that formed as a result of applying electric fields of sufficient strength to cause $\mathcal{S}$ to become unstable propagated to the right (in the direction of the electric field). The speed of propagation increased and the number of waves on $0 < x < l$ decreased with increasing E. Apart from this the picture is essentially the same for all cases, hence we illustrate this case with only a single contour plot (Figure 10) for $E = 5{\cdot}0$.

5. Discussion

Without the electric field the same general behaviour was found in all three cases (prescribed concentration, zero flux and periodic boundary conditions). In each case where there is at least one wavenumber lying between X_1 and X_2 (see Figures 1, 2a and Equation (20)) the spatially uniform steady state $\mathcal{S}$ is destabilised through a Turing bifurcation after an initial perturbation. This requires $D\mu^2 < 3 - 2\sqrt{2}$, otherwise $\mathcal{S}$ remains stable. In all cases a stable, spatially non-uniform steady state (pattern) is achieved at large times. The structure of this pattern reflects the values of the dimensionless parameters, namely D, μ and l, as well as the particular boundary conditions imposed. For periodic boundary conditions the pattern consists of a series of stationary waves of uniform frequency and amplitude, such that an exact number of waves are formed on the given interval. This is not necessarily the case with prescribed concentration and zero flux boundary conditions, where the form that the pattern takes can also depend on the location of the initial perturbation.

Applying electric fields to the system results in qualitatively different behaviour depending on the nature of the boundary conditions, essentially differentiating between the cases of periodic and prescribed concentration or zero flux boundary conditions. In the former case, the electric field causes the stationary pattern to change to a pattern propagating as a series of travelling waves. The speed of propagation, as well as the structure, of these travelling waves

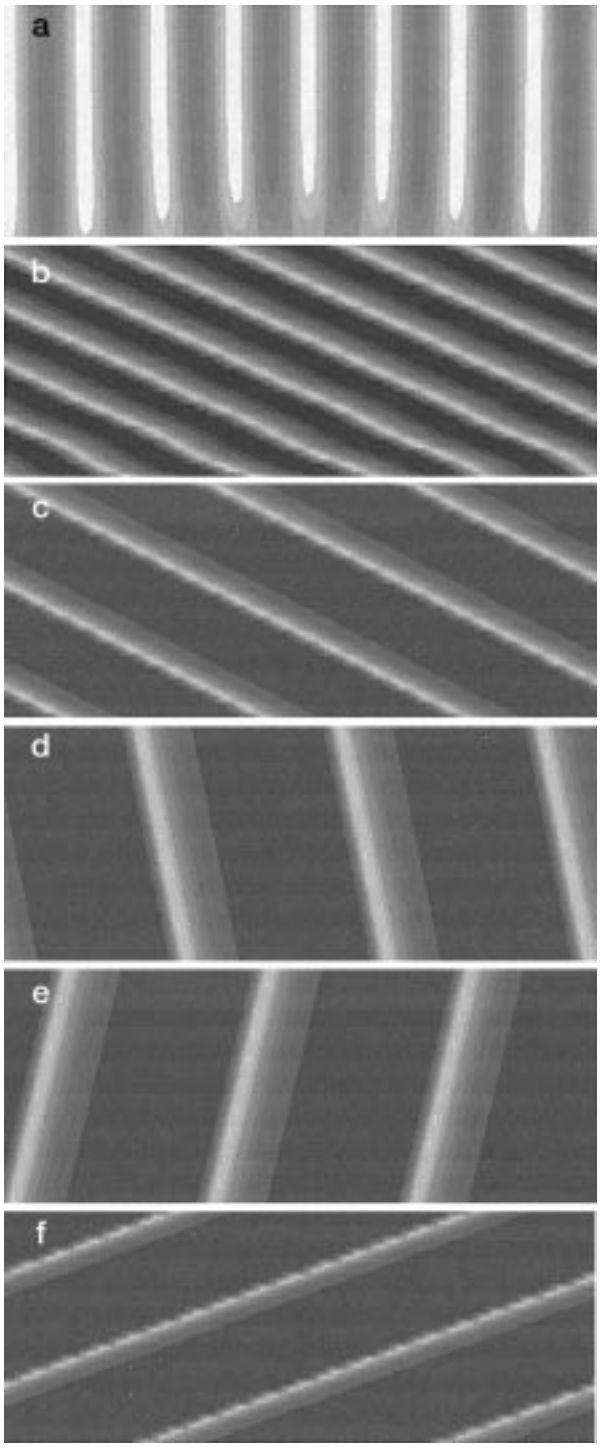

Figure 9. Grey-gevel contour plots of b obtained from the numerical integration of initial-boundary-value problem (4, 5, 10) (periodic conditions) for $\mu = 1{\cdot}5$, $D = 0{\cdot}0674$, $l = 20{\cdot}0$ and (a) $E = 0{\cdot}0$, (b) $E = 2{\cdot}828$, (c) $E = 6{\cdot}0$, (d) $E = 6{\cdot}8556$, (e) $E = 7{\cdot}071$, (f) $E = 11{\cdot}0$, the darker the colour the higher the concentration of B^+.

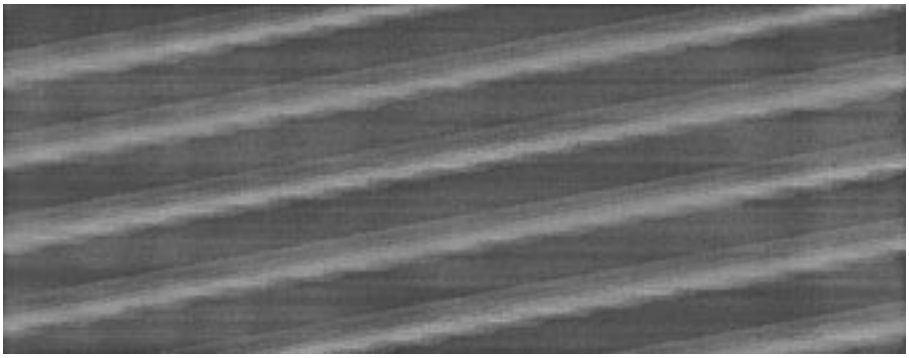

Figure 10. A grey-level contour plot of b obtained from the numerical integration of initial-boundary-value problem (4, 5, 10) (periodic conditions) for $\mu = 1{\cdot}5$, $D = 10{\cdot}0$, $l = 100{\cdot}0$ and $E = 5{\cdot}0$, the darker the colour the higher the concentration of B^+.

is strongly influenced by the the strength of the electric field; generally both the propagation speed and the wavelength of the waves increases as the field strength increases, though changes in propagation direction are also possible. These structures are not terminated and are seen to persist for all field strengths, giving rise to large propagation speeds in strong fields. A further feature to note for this case is that spatio-temporal behaviour can be generated even when none would be possible without the electric field, by applying a field above some minimum value.

This is not the case with prescribed concentration or zero flux boundary conditions, where a necessary condition for the generation of spatial structure is that the system parameters satisfy the basic conditions required for a Turing bifurcation. The behaviour in both these cases is qualitatively similar, in that the conditions from linear theory for $\mathcal{S}$ to become unstable are the same and that any patterns that are formed remain stationary when the electric field is applied. No long time unsteady behaviour was found in either case. Applying an electric field can change the basic pattern form (generally skewing it in the direction of the field), can give rise to patterns where the domain size is such that none would form without the field and can give multistability, with the pattern seen being dependent on the nature of the initial perturbation.

A further difference is that pattern formation can be suppressed by applying a sufficiently strong field. We illustrate this in Figure 11, where we give a grey-level contour plot of b, taking $D = 0{\cdot}05$, $l = 12{\cdot}0$, $\mu = 1{\cdot}5$ and zero flux boundary conditions. For this figure the system was first allowed to evolve (to $t = 350$) into the Turing pattern without the electric field being applied. At $t = 350$ a slowly increasing field strength was applied, $E = 0{\cdot}04(t - 350)$, to $t = 610$, where $E = 10{\cdot}4$ (above the value where patterns can exist). This figure shows the initially steady pattern increasing in amplitude and slowly propagating in the direction of the field, leaving the domain at the end $X = 1$. The result is the number of 'peaks' in the pattern decreasing as E increases (compare with the sequence of plots shown in Figures 4 and 7) with its system reverting to the spatially uniform state $\mathcal{S}$ at a sufficiently high field strength (by $E = 10$ in this case).

There is some experimental evidence [30] that applying electric fields can strongly affect Turing structures. These experiments show the development of a front when the field is applied, which propagates partially across the reactor leaving a region of spatial structure ahead separated from a region of uniform concentration. This behaviour is, in many respects, not dissimilar to the results shown in Figures 4e, 7e and 11. They also report that electric

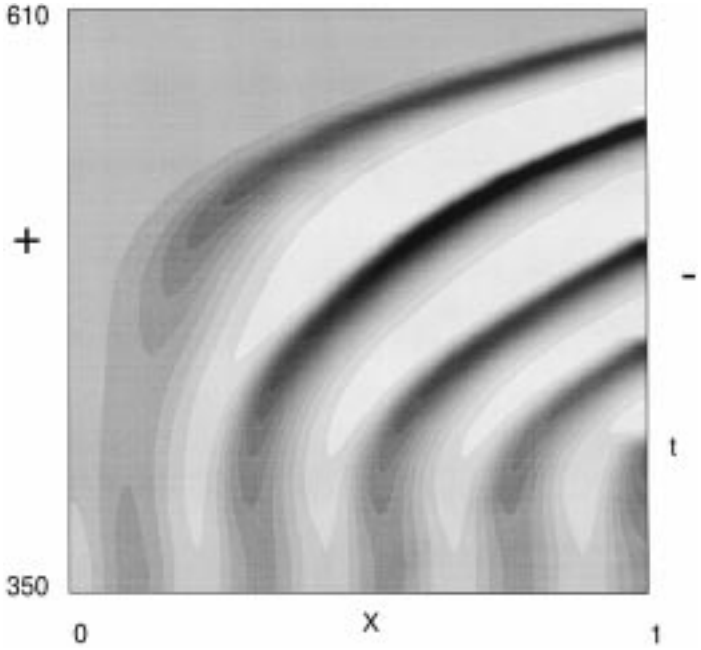

Figure 11. Effect of a slowly increasing electric field strength with zero-flux boundary conditions, the darker the colour the higher the concentration of B^+. Here $D = 0{\cdot}05$, $\mu = 1{\cdot}5$, $l = 12{\cdot}0$, a Turing pattern was allowed to develop fully (to $t = 350$) before the field was switched on, $E = 0{\cdot}04(t - 350)$. The spatially uniform state is achieved by $t = 600$, ($E = 10{\cdot}0$).

fields above some critical value remove all spatial structure, also in line with our theoretical predictions.

Finally, we note that our attention has been focussed entirely on the case when the kinetic model is stable (here $\mu > 1$). Our kinetic model is capable of an oscillatory response, arising through a supercritical Hopf bifurcation, and the interaction between this and the steady spatial structures generated by the electric field-influenced Turing bifurcations described above is under further investigation.

Acknowledgements

AF wishes to thank British Steel for their support.

References

1. H. Sevcikova, M. Marek and S.C. Muller, The reversal and splitting of waves in an excitable medium caused by an electric field. *Science* 257 (1992) 951–954.
2. H. Sevcikova, J. Kosek and M. Marek, Splitting of 2D waves of excitation in a direct current electric field. *J. Phys. Chem.* 100 (1996) 1666–1675.
3. J.J. Taboada, A.P. Munuzuri, V. Perez-Munuzuri, M. Gomez-Gesteira and V. Perez-Villar, Spiral break up induced by an electric current in a Belousov-Zhabotinsky medium. *Chaos* 4 (1994) 519–524.
4. S.C. Muller, O. Steinbock and J. Schutze, Autonomous pacemaker of chemical waves created by spiral annihilation. *Physica A* 188 (1992) 47–54.
5. O. Steinbock, J. Schutze and S. C. Muller, Electric-field-induced drift and deformation of spiral waves in an excitable medium. *Phys. Rev. Letters* 68 (1992) 248–251.

6. K.I. Agladze and P. DeKepper, Influence of electric field on rotating spiral waves in the Belousov-Zhabotinsky reaction. *J. Phys. Chem.* 96 (1992) 5239–5242.
7. J. Kosek, H. Sevcikova and M. Marek, Splitting of excitable pulse waves. *J. Phys. Chem.* 99 (1995) 6889–6896.
8. H. Sevcikova, I. Schreiber and M. Marek, Dynamics of oxidation Belousov-Zhabotinsky waves in an electric field. *J. Phys. Chem.* 100 (1996) 19153–19164.
9. H. Sevcikova and M. Marek, Chemical front waves in an electric field. *Physica D* 13 (1984) 379–386.
10. H. Sevcikova and M. Marek, Concentration pulses and fronts in electric fields. *J. Phys. Chem.* 88 (1984) 2181–2183.
11. H. Sevcikova, D. Snita and M. Marek, Reactions in microreactors in electric fields. In: W. Ehrfeld (ed.), *Proceedings of the First International Conference on Microreactor Technology*, Springer-Verlag (1997) pp. 46–54.
12. L. Forstova, H. Sevcikova, M. Marek and J.H. Merkin, Electric field effects on the local stoichiometry of front waves. *Chemical Engineering Science* 55 (2000) 391–431.
13. D. Snita, H. Sevcikova, M. Marek and J.H. Merkin, Ionic autocatalytic reaction fronts in electric fields. *J. Phys. Chem.* 100 (1996) 18740–18748.
14. D. Snita, H. Sevcikova, M. Marek and J.H. Merkin, Travelling waves in an ionic autocatalytic chemical system with an imposed electric field. *Proc. R. Soc. London* A453 (1997) 2325–2351.
15. D. Snita, H. Sevcikova, J. Lindner, M. Marek and J.H. Merkin, Capillary electrophoresis with chemical reaction. *J. Chem. Soc. Faraday Trans.* 94 (1998) 213–222.
16. J.H. Merkin, H. Sevcikova, D. Snita, M. Marek and J.H. Merkin, The effects of an electric field on an autocatalytic ionic reaction in a system with high ionic strength. *IMA J. Appl. Math.* 60 (1998) 1–31.
17. A.B. Finlayson and J.H. Merkin, Travelling waves in an ionic quadratic autocatalytic chemical system. *Math. Computer Modelling* 20 (1999) 89–112.
18. A.B. Rovinsky, A.M. Zhabotinsky and I.R. Epstein, Stability of planar reactive fronts in external fields. *Phys. Rev. E* 58 (1998) 5541–5547.
19. P. Ortoleva, Chemical wave-electric field interaction phenomena. *Physica D* 26 (1987) 67–84.
20. P. Hasal, A.F. Munster and M. Marek, Spatiotemporal chaos in an electric current driven ionic reaction-diffusion system. *Chaos* 4 (1994) 531–546.
21. A.F. Munster, P. Hasal, D. Snita and M. Marek, Charge distribution and electric field effects on spatiotemporal patterns. *Phys. Rev. E* 50 (1994) 546–550.
22. S. Schmidt and P. Ortleva, A new chemical wave equation for ionic systems. *J. Chem. Phys.* 67 (1977) 3771–3776.
23. D. Snita and M. Marek, Transport and reaction in ionic chemical systems. *Physica D* 75 (1994) 521–540.
24. P. Gray and S.K. Scott, *Chemical Oscillations and Instabilities: Non-Linear Chemical Kinetics*. Oxford: Oxford University Press (1990) 534 pp.
25. J.H. Merkin, D.J. Needham and S.K. Scott, Oscillatory chemical reactions in closed vessels. *Proc. R. Soc. London* A406 (1986) 299–323.
26. R. Hill, J.H. Merkin and D.J. Needham, Stable pattern and standing wave formation in a simple isothermal cubic autocatalytic reaction scheme. *J. Eng. Math.* 29 (1995) 423–436.
27. R.A. Satnoianu, J.H. Merkin and S.K. Scott, Differential-flow-induced instability in a cubic autocatalator system. *J. Eng. Math.* 33 (1998) 77–102.
28. R.A. Satnoianu, J.H. Merkin and S.K. Scott, Spatio-temporal structures in a differential flow reactor with cubic autocatalator kinetics. *Physica D* 124 (1998) 345–367.
29. J.H. Merkin and D.J. Needham, Propagating reaction-diffusion waves in a simple isothermal quadratic autocatalytic chemical system. *J. Eng. Math.* 23 (1989) 343–356.
30. A.F. Munster, S. Wolff, F. Fecher, Travelling waves induced by an electric field in the MBO-reaction. In preparation.